



# THE UNIVERSITY *of* EDINBURGH

## Edinburgh Research Explorer

### Retrieval of Elastodynamic Green's Functions through Single-Sided Marchenko Inverse Scattering

**Citation for published version:**

Curtis, A & Meles, G 2014, 'Retrieval of Elastodynamic Green's Functions through Single-Sided Marchenko Inverse Scattering' *Physical Review E - Statistical, Nonlinear and Soft Matter Physics*, vol. 90, no. 6.

**Link:**

[Link to publication record in Edinburgh Research Explorer](#)

**Document Version:**

Peer reviewed version

**Published In:**

*Physical Review E - Statistical, Nonlinear and Soft Matter Physics*

**General rights**

Copyright for the publications made accessible via the Edinburgh Research Explorer is retained by the author(s) and / or other copyright owners and it is a condition of accessing these publications that users recognise and abide by the legal requirements associated with these rights.

**Take down policy**

The University of Edinburgh has made every reasonable effort to ensure that Edinburgh Research Explorer content complies with UK legislation. If you believe that the public display of this file breaches copyright please contact [openaccess@ed.ac.uk](mailto:openaccess@ed.ac.uk) providing details, and we will remove access to the work immediately and investigate your claim.



# Retrieval of Elastodynamic Green's Functions through Single-Sided Marchenko Inverse Scattering

Carlos Alberto da Costa Filho,\* Matteo Ravasi, Andrew Curtis, and Giovanni Angelo Meles

*School of GeoSciences, University of Edinburgh,*

*Grant Institute, James Hutton Road,*

*Edinburgh EH9 3FE, United Kingdom*

## Abstract

The solution of the inverse scattering problem for the 1D Schrödinger equation is given by the Marchenko equation. Recently, a Marchenko-type equation has been derived for 3D acoustic wavefields, whose solution has been shown to recover the Green's functions from points within the medium to its exterior, using only single-sided scattered data. Here we extend this approach to 3D vectorial wavefields that satisfy the elastodynamic wave equation, and recover Green's functions from points interior to an elastic, solid-state medium from purely external and one-sided measurements. The method is demonstrated in a solid-Earth-like model to construct Green's functions using only subsurface sources, from Earth-surface force and deformation sources and particle velocity and stress measurements.

---

\* [c.costa@ed.ac.uk](mailto:c.costa@ed.ac.uk)

## I. INTRODUCTION

Three distinct but related wave scattering problems are commonly studied. First, inverse scattering methods estimate perturbations in medium properties from recorded scattered wavefields. One-dimensional inverse scattering is governed by the Gelfand-Levitan-Marchenko equation [1, 2], known simply as the Marchenko equation. This is an exact integral relating the scattered field measured on one side of the medium to its interior inhomogeneities.

The second problem is focusing—crafting an incident wavefield such that, at a certain time, the wavefield vanishes in all but one point of the medium [3].

A third class of problems is that of retrieving Green’s functions by wavefield interferometry [4–7]. This concerns the construction of the response that would have been recorded by a sensor at one point in a medium if an impulsive source had been placed at the location of another sensor.

While initially disjunct, these three problems have been shown to be closely related. Rose [8] showed that for the one-dimensional time-dependent Schrödinger equation, the Marchenko equation also governs the theory of focusing. Namely, scattered data from one side of the medium can be used to generate a wavefield that focuses only at an arbitrary point inside of the medium; the focused wavefield also satisfies the Marchenko equation. The technique is now known as single-sided autofocusing [8, 9].

Broggini and Snieder [10] demonstrated that these focused wavefields can be exploited to recover Green’s functions with a source at the focusing location, and Halliday and Curtis [11] showed how such Green’s functions are nonlinearly related to the scattering perturbations in the medium of the first problem class above.

The single-sided autofocusing method was extended to the 3D acoustic wave equation [12, 13], but to date has only been developed for scalar wavefields. Hence, it has no theoretical basis in solid-state media, or for intrinsically vectorial wavefields (e.g. elastic, electromagnetic, seismoelectric, electrokinetic).

We develop the autofocusing method for vector wavefields in 3D elastic media, showing that Green’s and focusing functions are related through a single-sided representation theorem, furthering our initial work [14, 15]. We refer to this method as elastic autofocusing. We derive the corresponding Marchenko equation and an iterative solution which creates an

elastic wavefield that focuses at an arbitrary point in the medium; the Green’s function with source at that point is recovered from the focused wavefield. That is to say, we provide a theoretical framework valid for lossless 3D elastic media that allows the Green’s function from a virtual source interior to the medium to the surface to be recovered. Moreover, we require only the scattered data measured at the surface and an estimate of the direct wave from the virtual source to the surface. Thus, while usual data-driven interferometric retrieval of Green’s functions methods [4, 5, 16–18] require sources or receivers on full boundaries around or throughout the medium, and the physical presence of a receiver or source at the focusing position, autofocusing requires none of these.

The focusing of ultrasonic acoustic wavefields has been applied for such purposes as medical lithotripsy (the destruction of gall bladders or kidney stones) [19], brain cancer treatment [20] and nondestructive testing [21]. In these applications data can be acquired all around the target medium. In studying the interior of the Earth this is not often possible, and single-sided seismic elastic wave data must be used for imaging subsurface heterogeneities. While autofocusing has been applied to acoustic (fluid) Earth models [22, 23] this work provides a more realistic framework to treat real (solid) Earth applications. It also develops the first derivation of autofocusing for vectorial wavefields, opening possibilities to adapt it to other wave phenomena e.g. electromagnetism.

## II. THEORY

### A. Green’s and focusing functions

In this section we introduce quantities and relations necessary for the development of elastic autofocusing theory. We consider the following solid model: a lossless elastic medium that is inhomogeneous, anisotropic and arbitrarily complex below a certain depth ( $z < z_0$ ), but homogenous above it (Fig. 1a). This medium is characterized by its density  $\rho(\mathbf{x})$  and stiffness tensor  $c_{ijkl}(\mathbf{x})$  at location  $\mathbf{x}$ . External sources of volume force density or deformation rate density, when placed in such a medium, induce linear wave motion described by the elastodynamic wave equation in the space-frequency domain:

$$\partial_j c_{ijkl}(\mathbf{x}) \{ \partial_l v_k(\mathbf{x}, \omega) - h_{kl}(\mathbf{x}, \omega) \} + \omega^2 \rho(\mathbf{x}) v_i(\mathbf{x}, \omega) = \omega f_i(\mathbf{x}, \omega) \quad (1)$$

where indices  $i, j, k$  and  $l$  may be  $x$  or  $y$  for the horizontal coordinates and  $z$  for the vertical coordinate. Einstein notation is used implying summation over repeated indices, indices on partial derivatives indicate direction over which the derivative is taken, and  $\iota$  represents the imaginary unit. The observed quantity is the particle velocity (time derivative of the particle displacement) represented in the space-frequency domain as  $v(\mathbf{x}, \omega)$ , and  $f_i$  and  $h_{ij}$  represent force and deformation sources respectively.

If one of  $f$  or  $h$  is a delta function in the  $p$  or  $pq$  direction respectively, and the other is null, we refer to the solutions of the resulting equation as Green's functions, and denote them by  $G_{(i,q)}^{(v,f)}(\mathbf{x}, \mathbf{x}_0'', \omega)$  or  $G_{(i,pq)}^{(v,h)}(\mathbf{x}, \mathbf{x}_0'', \omega)$  respectively. Green's function superscripts represent the observed quantity and source type, and subscripts the selected receiver and source components, respectively; its arguments, from left to right, are observation position, which can be anywhere in the medium, source position (specified below) and angular frequency. From the generalized Hooke's law in the frequency domain [24, 25],

$$\iota\omega\tau_{ij} - c_{ijkl}\partial_l v_k = 0 \quad (2)$$

we may define

$$G_{(ij,\cdot)}^{(\tau,\cdot)}(\mathbf{x}_0, \mathbf{x}_0'', \omega) = (\iota\omega)^{-1} c_{ijkl}(\mathbf{x}) \partial_l G_{(k,\cdot)}^{(v,\cdot)}(\mathbf{x}, \mathbf{x}_0'', \omega) \quad (3)$$

Waves often have directivity, that is, a direction in which most of its energy travels. For example, in relation to quantum scattering, it is common to study incoming and outgoing waves separately, though they are both parts of the Green's function of the Schrödinger equation. Similarly, so called one-way wavefield decompositions separate the full wavefield into components that travel up or down along (herein) the vertical  $z$ -axis. First developed for acoustic wavefields in homogenous media [26], they have been extended to electromagnetic and elastic wavefields in layered media [27]. Here we apply a decomposition for arbitrarily inhomogeneous anisotropic elastic media [28] to the Green's function at the receiver location  $\mathbf{x}_0$  along  $\partial\mathbb{D}_0$ .

A consequence of homogeneity of the medium above surface  $\partial\mathbb{D}_0$  is that it is nonreflecting; that is, waves propagating upwards above  $\partial\mathbb{D}_0$  do not return, implying that the down-going velocity field at the surface vanishes. This condition, combined with the elastic Rayleigh I integral [28], yields an expression for the particle stress at  $\partial\mathbb{D}_0$ :

$$G_{(iz,q)}^{+(\tau,f)}(\mathbf{x}_0, \mathbf{x}_0'', \omega) \Big|_{\mathbf{x}_0 \in \partial\mathbb{D}_0} = -\frac{1}{2} \delta_{iq} \delta(\mathbf{x}_0 - \mathbf{x}_0'') \quad (4)$$

where  $\delta_{iq}$  is the Kronecker delta,  $\delta(\mathbf{x}_0 - \mathbf{x}_0'')$  is the Dirac delta, and the superscript “+” denotes the down-going field component; subsequently “-” will be used for the up-going component.

The source-free one-dimensional Schrödinger equation admits so called fundamental solutions, which reduce to  $e^{\pm ikx}$  as  $x$  approaches  $\pm\infty$  [29]. They are useful for the derivation of Marchenko-type solutions of the 1D Schrödinger equation. As has been shown in [13], these types of solutions are also present in the study of the Marchenko-type equations for the three-dimensional acoustic wave equation. In acoustics, they are noncausal solutions of the source-free wave equation that propagate in such a way that at  $t = 0$  they collapse to a delta function at a certain spatial point, and subsequently diverge [23]. Therefore, it proves useful to define similar functions in the case of elastic media.

We consider a region  $\mathbb{D}$  of the medium bounded by two transparent planes  $\partial\mathbb{D}_0$  and  $\partial\mathbb{D}_m$  at respective depth levels  $z_0$  and  $z_m$ . A reference medium is defined as being identical to the true solid medium where  $G$  is defined, but is nonreflecting and homogenous below  $z_m$  (Fig. 1b). It is important to note that this is not the true medium, but simply a reference medium that coincides with the true medium inside  $\mathbb{D}$ . We impose that the focusing function satisfies the source-free version of the elastodynamic wave equation in Eq. (1) in the reference medium, and at  $t = 0$  must collapse to a unidirectional force density delta function at  $\mathbf{x}'_m$ :

$$F_{(iz,p)}^{+(\tau,f)}(\mathbf{x}_m, \mathbf{x}'_m, \omega)|_{\mathbf{x}_m \in \partial\mathbb{D}_m} = -\frac{1}{2}\delta_{ip}\delta(\mathbf{x}_m - \mathbf{x}'_m) \quad (5)$$

where  $\mathbf{x}_m$  and  $\mathbf{x}'_m$  are both on the same plane  $\partial\mathbb{D}_m$ .

## B. Green’s function representation

We now develop an integral relationship between the Green’s functions from sources inside  $\mathbb{D}$ , to Green’s functions with sources outside of it, as well as to the focusing functions. This is a vital step in the derivation of the three-dimensional elastodynamic Marchenko equation.

Consider two wavefield states  $A$  and  $B$ , to be made explicit shortly, defined to be sourceless in the closed subregion  $\mathbb{D}_c$  of  $\mathbb{D}$ . The elastodynamic reciprocity theorems hold for these

two states [7]:

$$\oint_{\partial\mathbb{D}_c} \{v_i^B \tau_{ij}^A - \tau_{ij}^B v_i^A\} n_j d^2\mathbf{x} = 0 \quad (6)$$

$$\oint_{\partial\mathbb{D}_c} \{v_i^B (\tau_{ij}^A)^* + \tau_{ij}^B (v_i^A)^*\} n_j d^2\mathbf{x} = 0 \quad (7)$$

where  $n_j$  is the outward-pointing vector normal to closed surface  $\partial\mathbb{D}_c$ ,  $v_i^A$  and  $v_i^B$  represent the velocities of states  $A$  and  $B$ , and  $\tau_{ij}^A$  and  $\tau_{ij}^B$  their associated stresses.

Given suitable radiation conditions [30], the area of integration may be expanded to encompass the whole region  $\mathbb{D}$ . Then,  $\partial\mathbb{D} = \partial\mathbb{D}_0 \cup \partial\mathbb{D}_m$  assuming the medium is sufficiently extensive horizontally that the contribution to integrals in Eqs. (6) and (7) from sections of  $\partial\mathbb{D}_c$  on the sides of the model is negligible. The outward normals then become opposing vertical vectors yielding

$$\oint_{\partial\mathbb{D}_0} \{v_i^B \tau_{iz}^A - \tau_{iz}^B v_i^A\} d^2\mathbf{x}_0 = \oint_{\partial\mathbb{D}_m} \{v_i^B \tau_{iz}^A - \tau_{iz}^B v_i^A\} d^2\mathbf{x}_m \quad (8)$$

$$\oint_{\partial\mathbb{D}_0} \{v_i^B (\tau_{ij}^A)^* + \tau_{ij}^B (v_i^A)^*\} d^2\mathbf{x}_0 = \oint_{\partial\mathbb{D}_m} \{v_i^B (\tau_{iz}^A)^* + \tau_{iz}^B (v_i^A)^*\} d^2\mathbf{x}_m \quad (9)$$

The fields in Eqs. (8) and (9) can be separated into up- and down-going components, assuming that no evanescent waves are present in the wavefields at the location of the decomposition:

$$\begin{aligned} \oint_{\partial\mathbb{D}_0} \{(v_i^{B+} + v_i^{B-})(\tau_{iz}^{A+} + \tau_{iz}^{A-}) - (\tau_{iz}^{B+} + \tau_{iz}^{B-})(v_i^{A+} + v_i^{A-})\} d^2\mathbf{x}_0 = \\ \oint_{\partial\mathbb{D}_m} \{v_i^{B+} + v_i^{B-})(\tau_{iz}^{A+} + \tau_{iz}^{A-}) - (\tau_{iz}^{B+} + \tau_{iz}^{B-})(v_i^{A+} + v_i^{A-})\} d^2\mathbf{x}_m \quad (10) \end{aligned}$$

$$\begin{aligned} \oint_{\partial\mathbb{D}_0} \{(v_i^{B+} + v_i^{B-})(\tau_{iz}^{A+} + \tau_{iz}^{A-})^* + (\tau_{iz}^{B+} + \tau_{iz}^{B-})(v_i^{A+} + v_i^{A-})^*\} d^2\mathbf{x}_0 = \\ \oint_{\partial\mathbb{D}_m} \{v_i^{B+} + v_i^{B-})(\tau_{iz}^{A+} + \tau_{iz}^{A-})^* + (\tau_{iz}^{B+} + \tau_{iz}^{B-})(v_i^{A+} + v_i^{A-})^*\} d^2\mathbf{x}_m \quad (11) \end{aligned}$$

The integrals in Eqs. (10) and (11) can be simplified by considering the contributions of each combination of up- and down-going component. In Eq. (10) the integral of terms

which combine the same direction e.g.  $v_i^{B+}\tau_{iz}^{A+}$  is the negative of the integral of the terms combining the opposing directions e.g.  $\tau_{iz}^{B-}v_i^{A-}$ , thus canceling the contributions of these terms [28]. Similarly, in Eq. (11) the integrals which cancel each other are those arising from terms which combine fields with opposing directions, e.g. the integral of  $v_i^{B+}(\tau_{iz}^{A-})^*$  cancels that of  $\tau_{iz}^{B-}(v_i^{A+})^*$ . Furthermore, on the left-hand side of Eq. (10) the term  $v_i^{B+}\tau_{iz}^{A-}$  contributes the same energy as  $-\tau_{iz}^{B-}v_i^{A+}$ , that is, their integrals over the surface  $\partial\mathbb{D}_0$  are the same [28]. On its right-hand side, within the integral over  $\partial\mathbb{D}_m$ , the equivalent is valid for the terms  $v_i^{B-}\tau_{iz}^{A+}$  and  $-\tau_{iz}^{B-}v_i^{A+}$ , as well as for  $v_i^{B+}\tau_{iz}^{A-}$  and  $-\tau_{iz}^{B+}v_i^{A-}$ , simplifying the previous expression considerably:

$$\int_{\partial\mathbb{D}_0} \{v_i^{B-}\tau_{iz}^{A+} - \tau_{iz}^{B-}v_i^{A+} - 2\tau_{iz}^{B+}v_i^{A-}\} d^2\mathbf{x}_0 = \int_{\partial\mathbb{D}_m} 2\{v_i^{B-}\tau_{iz}^{A+} - \tau_{iz}^{B+}v_i^{A-}\} d^2\mathbf{x}_m \quad (12)$$

The equivalent quantities for Eq. (11) are  $v_i^{B+}(\tau_{iz}^{A+})^*$  and  $\tau_{iz}^{B+}(v_i^{A+})^*$ , as well as  $v_i^{B-}(\tau_{iz}^{A-})^*$  and  $\tau_{iz}^{B-}(v_i^{A-})^*$ , yielding

$$\int_{\partial\mathbb{D}_0} \{v_i^{B-}(\tau_{iz}^{A-})^* + \tau_{iz}^{B-}(v_i^{A-})^* + 2\tau_{iz}^{B+}(v_i^{A+})^*\} d^2\mathbf{x}_0 = \int_{\partial\mathbb{D}_m} 2\{v_i^{B+}(\tau_{iz}^{A+})^* + \tau_{iz}^{B-}(v_i^{A-})^*\} d^2\mathbf{x}_m \quad (13)$$

Now we substitute the quantities of state  $A$  and  $B$  for those of the previously defined focusing function  $F_{(\cdot,p)}^{(\cdot,f)}(\mathbf{x}, \mathbf{x}'_m, \omega)$  and the Green's function  $G_{(\cdot,q)}^{(\cdot,f)}(\mathbf{x}, \mathbf{x}''_0, \omega)$ , respectively. We recall that  $F$  has no up-going velocity field at  $\partial\mathbb{D}_m$ ; therefore on both right-hand sides of Eqs. (12) and (13), the terms containing  $v_i^{A-}$  vanish. Once the conditions of Eqs. (4) and (5) are applied to Eqs. (12) and (13), expressions that relate the up- and down-going Green's functions to focusing functions are obtained:

$$G_{(p,q)}^{-(v,f)}(\mathbf{x}'_m, \mathbf{x}''_0, \omega) = -F_{(q,p)}^{-(v,f)}(\mathbf{x}''_0, \mathbf{x}'_m, \omega) + \int_{\partial\mathbb{D}_0} \{G_{(iz,q)}^{-(\tau,f)}(\mathbf{x}_0, \mathbf{x}''_0, \omega)F_{(i,p)}^{+(v,f)}(\mathbf{x}_0, \mathbf{x}'_m, \omega) - G_{(i,q)}^{-(v,f)}(\mathbf{x}_0, \mathbf{x}''_0, \omega)F_{(iz,p)}^{+(\tau,f)}(\mathbf{x}_0, \mathbf{x}'_m, \omega)\} d^2\mathbf{x}_0 \quad (14)$$

$$G_{(p,q)}^{+(v,f)}(\mathbf{x}'_m, \mathbf{x}''_0, \omega) = F_{(q,p)}^{+(v,f)*}(\mathbf{x}''_0, \mathbf{x}'_m, \omega) - \int_{\partial\mathbb{D}_0} \{G_{(i,q)}^{-(v,f)}(\mathbf{x}_0, \mathbf{x}''_0, \omega)F_{(iz,p)}^{-(\tau,f)*}(\mathbf{x}_0, \mathbf{x}'_m, \omega) + G_{(iz,q)}^{-(\tau,f)}(\mathbf{x}_0, \mathbf{x}''_0, \omega)F_{(i,p)}^{-(v,f)*}(\mathbf{x}_0, \mathbf{x}'_m, \omega)\} d^2\mathbf{x}_0 \quad (15)$$

We sum Eqs. (14) and (15), and apply elastodynamic reciprocity theorems in [7] which state that  $G_{(i,j)}^{(v,f)}(\mathbf{x}, \mathbf{x}', \omega) = G_{(j,i)}^{(v,f)}(\mathbf{x}', \mathbf{x}, \omega)$  and  $G_{(ij,k)}^{(\tau,f)}(\mathbf{x}, \mathbf{x}', \omega) = G_{(k,ij)}^{(v,h)}(\mathbf{x}', \mathbf{x}, \omega)$ . An auxiliary



function given by

$$H_{(j,p)}^{(v,f)}(\mathbf{x}, \mathbf{x}'_m, \omega) = F_{(j,p)}^{+(v,f)}(\mathbf{x}, \mathbf{x}'_m, \omega) - F_{(j,p)}^{-(v,f)*}(\mathbf{x}, \mathbf{x}'_m, \omega) \quad (16)$$

can then be used to obtain a simpler representation of the velocity Green's function in terms of focusing functions:

$$G_{(q,p)}^{(v,f)}(\mathbf{x}''_0, \mathbf{x}'_m, \omega) = H_{(q,p)}^{(v,f)*}(\mathbf{x}''_0, \mathbf{x}'_m, \omega) + \int_{\partial\mathbb{D}_0} \left\{ G_{(q,iz)}^{-(v,h)}(\mathbf{x}''_0, \mathbf{x}_0, \omega) H_{(i,p)}^{(v,f)}(\mathbf{x}_0, \mathbf{x}'_m, \omega) - G_{(q,i)}^{-(v,f)}(\mathbf{x}''_0, \mathbf{x}_0, \omega) H_{(iz,p)}^{(\tau,f)}(\mathbf{x}_0, \mathbf{x}'_m, \omega) \right\} d^2\mathbf{x}_0 \quad (17)$$

By applying the generalized Hooke's law in Eq. (2) to Eqs. (16) and (17), we obtain

$$G_{(kl,p)}^{(\tau,f)}(\mathbf{x}''_0, \mathbf{x}'_m, \omega) = -H_{(kl,p)}^{(\tau,f)*}(\mathbf{x}''_0, \mathbf{x}'_m, \omega) + \int_{\partial\mathbb{D}_0} \left\{ G_{(kl,iz)}^{-(\tau,h)}(\mathbf{x}''_0, \mathbf{x}_0, \omega) H_{(i,p)}^{(v,f)}(\mathbf{x}_0, \mathbf{x}'_m, \omega) - G_{(kl,i)}^{-(\tau,f)}(\mathbf{x}''_0, \mathbf{x}_0, \omega) H_{(iz,p)}^{(\tau,f)}(\mathbf{x}_0, \mathbf{x}'_m, \omega) \right\} d^2\mathbf{x}_0 \quad (18)$$

By defining

$$\underline{\mathbf{G}}_{(p)}^{(f)} = \left( G_{(x,p)}^{(v,f)} \quad G_{(y,p)}^{(v,f)} \quad G_{(z,p)}^{(v,f)} \quad G_{(xz,p)}^{(\tau,f)} \quad G_{(yz,p)}^{(\tau,f)} \quad G_{(zz,p)}^{(\tau,f)} \right)^T$$

$$\underline{\mathbf{H}}_{(p)}^{(f)} = \left( H_{(x,p)}^{(v,f)} \quad H_{(y,p)}^{(v,f)} \quad H_{(z,p)}^{(v,f)} \quad -H_{(xz,p)}^{(\tau,f)} \quad -H_{(yz,p)}^{(\tau,f)} \quad -H_{(zz,p)}^{(\tau,f)} \right)^T$$

and

$$\underline{\mathbf{G}}^- = \begin{bmatrix} G_{(x,xz)}^{-(v,h)} & G_{(x,yz)}^{-(v,h)} & G_{(x,zz)}^{-(v,h)} & G_{(x,x)}^{-(v,f)} & G_{(x,y)}^{-(v,f)} & G_{(x,z)}^{-(v,f)} \\ G_{(y,xz)}^{-(v,h)} & G_{(y,yz)}^{-(v,h)} & G_{(y,zz)}^{-(v,h)} & G_{(y,x)}^{-(v,f)} & G_{(y,y)}^{-(v,f)} & G_{(y,z)}^{-(v,f)} \\ G_{(z,xz)}^{-(v,h)} & G_{(z,yz)}^{-(v,h)} & G_{(z,zz)}^{-(v,h)} & G_{(z,x)}^{-(v,f)} & G_{(z,y)}^{-(v,f)} & G_{(z,z)}^{-(v,f)} \\ G_{(xz,xz)}^{-(\tau,h)} & G_{(xz,yz)}^{-(\tau,h)} & G_{(xz,zz)}^{-(\tau,h)} & G_{(xz,x)}^{-(\tau,f)} & G_{(xz,y)}^{-(\tau,f)} & G_{(xz,z)}^{-(\tau,f)} \\ G_{(yz,xz)}^{-(\tau,h)} & G_{(yz,yz)}^{-(\tau,h)} & G_{(yz,zz)}^{-(\tau,h)} & G_{(yz,x)}^{-(\tau,f)} & G_{(yz,y)}^{-(\tau,f)} & G_{(yz,z)}^{-(\tau,f)} \\ G_{(zz,xz)}^{-(\tau,h)} & G_{(zz,yz)}^{-(\tau,h)} & G_{(zz,zz)}^{-(\tau,h)} & G_{(zz,x)}^{-(\tau,f)} & G_{(zz,y)}^{-(\tau,f)} & G_{(zz,z)}^{-(\tau,f)} \end{bmatrix}$$

we condense Eqs. (17) and (18) into one matrix equation. After applying an inverse Fourier transform defined by  $f(t) = (2\pi)^{-1} \int_{-\infty}^{\infty} \hat{f}(\omega) e^{-i\omega t} d\omega$  we obtain the following equation in the time domain:

$$\underline{\mathbf{G}}_{(p)}^{(f)}(\mathbf{x}''_0, \mathbf{x}'_m, t) = \underline{\mathbf{H}}_{(p)}^{(f)}(\mathbf{x}''_0, \mathbf{x}'_m, -t) + \int_{\partial\mathbb{D}_0} \int_{-\infty}^{\infty} \underline{\mathbf{G}}^-(\mathbf{x}''_0, \mathbf{x}_0, t - \tau) \underline{\mathbf{H}}_{(p)}^{(f)}(\mathbf{x}_0, \mathbf{x}'_m, \tau) d\tau d^2\mathbf{x}_0 \quad (19)$$

where we have used the same symbols for the function and its Fourier transform, using their arguments to differentiate one another.

### C. 3D elastodynamic Marchenko equation

The result obtained in Eq. (19) now contains the Green's function that we seek on the left-hand side. It requires the up-going (reflected) field  $\underline{\mathbf{G}}^-$  from surface sources and measured at the surface, as well as knowledge of the focusing functions in  $\underline{\mathbf{H}}$ , which are not known a priori. In effect, the aim of the autofocusing schema is to estimate these functions.

An argument using the reciprocity theorems for  $H$  and  $F$  shows that  $H$  is also a focusing function, but which focuses on the surface (its location is indicated by the second argument of the function). For single-sided autofocusing, Rose [8] assumes that it is composed of a delta function as a first arrival, followed by a coda which contains all scattered energy. Wapenaar et al. [13] therefore propose an ansatz for the shape of  $H$  in 3D acoustic autofocusing, which consists of a time-reversed direct (non-scattered) wave, and a scattered coda which arrives after the direct wave. However, while in acoustic media only pressure ( $P$ ) waves exist, body-wave propagation in elastic media also exhibits shear waves of different traverse polarization states ( $SH$  for horizontal polarization,  $SV$  for vertical), that travel at a different speeds than  $P$ -waves. Consequently, an arbitrary force density source will transmit not only  $P$ ,  $SH$  and  $SV$  direct arrivals, but also their conversions from one to another. To overcome this hurdle, we modify the previous equations to use  $P$ -,  $SV$ -, and  $SH$ -potentials (denoted by a  $\phi$  source instead of force density sources), by applying the appropriate differential operators [28] throughout Eq. (19). It is important to note that this assumes that the medium can be considered locally isotropic around  $\mathbf{x}'_m$ . Furthermore, we denote the travel time of the first arrival of the  $N$ -wave (denoting  $P$ -,  $SH$ - or  $SV$ -wave) at  $\mathbf{x}''_0$  from a source at  $\mathbf{x}'_m$  as  $t_d^N(\mathbf{x}''_0, \mathbf{x}'_m)$ , and assume that  $\underline{\mathbf{H}}_{(N)}^{(\phi)}(\mathbf{x}'_m, \mathbf{x}''_0, t)$  is composed of a direct wave propagating from  $\mathbf{x}'_m$  to  $\mathbf{x}''_0$ , and a subsequent scattered coda:

$$\underline{\mathbf{H}}_{(N)}^{(\phi)}(\mathbf{x}''_0, \mathbf{x}'_m, t) = \underline{\mathbf{G}}_{(N)}^{0(\phi)}(\mathbf{x}''_0, \mathbf{x}'_m, -t) + \theta(t + t_d^N(\mathbf{x}''_0, \mathbf{x}'_m)) \underline{\mathbf{M}}_{(N)}^{(\phi)}(\mathbf{x}''_0, \mathbf{x}'_m, t) \quad (20)$$

Here  $\theta$  is the Heaviside function, and superscript 0 denotes non-scattered component of the Green's function. Physically, Eq. (20) contains a direct wave pulse that travels forwards in time to focus at  $\mathbf{x}''_0$  at  $t = 0$  represented by  $\underline{\mathbf{G}}_{(N)}^{0(\phi)}$ . In a scattering medium this pulse is scattered as it travels, which would result in an imperfect focus at  $t = 0$ ; the term  $\underline{\mathbf{M}}_{(N)}^{(\phi)}$  must therefore guarantee that the effect of scattering is annulled, so as to achieve focusing only at  $\mathbf{x}''_0$  at  $t = 0$ .

After applying the ansatz of Eq. (20) and evaluating Eq. (19) at times before the first arrival  $t_d^N(\mathbf{x}_0'', \mathbf{x}'_m)$ , the 3D elastodynamic Marchenko equation is obtained:

$$0 = \int_{\partial\mathbb{D}_0} \int_{-\infty}^{\infty} \underline{\mathbf{G}}^-(\mathbf{x}_0'', \mathbf{x}_0, t - \tau) \underline{\mathbf{G}}_{(N)}^{0(\phi)}(\mathbf{x}_0, \mathbf{x}'_m, -\tau) d\tau d^2\mathbf{x}_0 + \int_{\partial\mathbb{D}_0} \int_{-t_d^N}^{\infty} \underline{\mathbf{G}}^-(\mathbf{x}_0'', \mathbf{x}_0, t - \tau) \underline{\mathbf{M}}_{(N)}^{(\phi)}(\mathbf{x}_0, \mathbf{x}'_m, \tau) d\tau d^2\mathbf{x}_0 + \underline{\mathbf{M}}_{(N)}^{(\phi)}(\mathbf{x}_0'', \mathbf{x}'_m, -t) \quad (21)$$

#### D. 3D elastic autofocusing

Previous autofocusing schemes solve the Marchenko equation by designing up- and down-going fields that, when combined in a specific form, yield the Green's function from a virtual source position in the subsurface. Based on [8, 9, 12] we derive an iterative scheme that solves the 3D elastodynamic Marchenko equation, and show how the Green's function can be recovered. The scheme defines two fields  $\underline{\mathbf{E}}_k^+$  and  $\underline{\mathbf{E}}_k^-$  that are iterated for  $k \geq 0$  using their respective relations in Eqs. (22) and (23). By initializing  $\underline{\mathbf{E}}_{-1}^- = \mathbf{0}$ , we define:

$$\underline{\mathbf{E}}_k^+(\mathbf{x}_0, \mathbf{x}_F, t) = \underline{\mathbf{G}}_{(N)}^{0(\phi)}(\mathbf{x}_0, \mathbf{x}_F, -t) - \theta(t + t_d^N(\mathbf{x}_0, \mathbf{x}_F)) \underline{\mathbf{E}}_{k-1}^-(\mathbf{x}_0, \mathbf{x}_F, -t) \quad (22)$$

$$\underline{\mathbf{E}}_k^-(\mathbf{x}_0'', \mathbf{x}_F, t) = \int_{\partial\mathbb{D}_0} \int_{-\infty}^{\infty} \underline{\mathbf{G}}^-(\mathbf{x}_0'', \mathbf{x}_0, t - \tau) \underline{\mathbf{E}}_k^+(\mathbf{x}_0, \mathbf{x}_F, \tau) d\tau d\mathbf{x}_0 \quad (23)$$

In the case of convergence we may drop the subscript  $k$  and substitute Eq. (22) into Eq. (23); for  $t < t_d^N(\mathbf{x}_0'', \mathbf{x}_F)$  the relation obtained thus is the Marchenko integral in Eq. (21), with

$$\underline{\mathbf{E}}_k^-(\mathbf{x}_0'', \mathbf{x}_F, t) = -\underline{\mathbf{M}}_{(N)}^{(\phi)}(\mathbf{x}_0'', \mathbf{x}_F, -t) \quad (24)$$

This relationship between the up- and down-going fields therefore yields a way to recover the Green's function with a source at  $\mathbf{x}_F$  based on Eq. (19). By substituting Eq. (24) into Eq. (22), and its result into Eq. (20), Eq. (21) can be reformulated to become an estimate of the Green's functions:

$$\tilde{\underline{\mathbf{G}}}_{(N)}^{(\phi)}(\mathbf{x}_0'', \mathbf{x}_F, t) = \underline{\mathbf{E}}^+(\mathbf{x}_0'', \mathbf{x}_F, -t) + \underline{\mathbf{E}}^-(\mathbf{x}_0'', \mathbf{x}_F, t). \quad (25)$$

We also observe that the step in Eq. (23) is the exact elastic receiver-side wavefield extrapolation integral used in elastic imaging [31], the elastic version of equivalent acoustic integrals

in [11]; the iterative scheme therefore consists of successive wavefield extrapolations of the relevant quantities given above. This shows quite clearly that, given an estimate of the direct wave from a point internal to the medium to points on its surface ( $\underline{\mathbf{G}}^0$  in Eq. (20)), and the scattered wavefield from and to same that surface ( $\underline{\mathbf{G}}^-$  in Eq. (19)), one may craft a focusing wavefield through the iterative application of wavefield extrapolations, in order to obtain the full internal Green’s function. A stationary phase analysis of the first iterations of this algorithm is provided in the Appendix, and is used to illustrate how waves that underwent conversions can be recovered through the algorithm.

### III. NUMERICAL RESULTS

A 2D numerical experiment using an inhomogeneous solid-Earth-like elastic medium is used to illustrate the method in a setup similar to that used for Geophysical imaging [13]. Figure 2 depicts the density distribution of the model. The  $P$ - and  $S$ -wave speeds are constant at 2.7 km/s and 1.5 km/s, respectively. Absorbing boundary conditions were applied at the top of the model, ensuring that no downward reflections occur at the top surface as required by the theory above. Figure 2 represents the virtual source position  $\mathbf{x}_F$  and the 201 source and receiver positions used to obtain the reflected data in  $\underline{\mathbf{G}}^-$ . Two separate autofocusing schemes are employed for  $P$ - and  $S$ - waves individually, and in both the direct transmissions  $\underline{\mathbf{G}}_{(N)}^{0(\phi)}$  were modeled in a smoothed version of the medium: the  $v_z$  component of the transmission for  $P$ -wave autofocusing is shown in Fig. 3a, the  $v_x$  component of the  $S$ -wave transmission in Fig. 3b. However, for both schemes, all recorded wavefield components are used.

These direct arrivals are time-reversed to initialize their respective  $\underline{\mathbf{E}}_0^+$  using Eq. (22). The reflected data  $\underline{\mathbf{G}}^-$  used is the data recorded between top-surface sources and receivers, without the direct-wave component, which is down-going (Fig. 3c).

Figures 4 and 5 show the results after running each autofocusing scheme for 10 iterations. Figure 4a shows  $v_z$  components constructed from  $P$ -wave autofocusing, and Fig. 4b  $v_z$  component responses modeled directly from a  $P$ -wave source. Figure 5 shows  $v_x$  components from  $S$ -wave autofocusing and directly modeled  $v_x$  responses from an  $S$ -wave source. Figures 6 and 7 show wave arrivals at a single receiver location. The black lines in Figs. 6 and 7 depict the true arrivals, and the pink (light gray) lines the ones recovered by autofocusing.

In both the  $P$ - and  $S$ -wave autofocusing, the results show that a large proportion of arrivals were recovered with the correct kinematics. Some of these recovered events are outlined with the dashed white lines in Figs. 4 and 5. They depict clearly, how even more complex wave arrivals due to the synclinal interface are recovered (first dashed white line with apex after 0.5s in Fig. 4). Although only  $v_z$  and  $v_x$  components are shown, components  $\tau_{zz}$  and  $\tau_{zx}$  were also recovered with similar accuracy. However, not every arrival was properly recovered, as shown by the dashed black lines in Figs. 4 and 5. Figure 4 exhibits one such arrival that fails to be accurately reconstructed. This event is a direct (nonscattered)  $P$ - $S$  converted transmission. In the near offset it appears well reconstructed, but does not appear in the farther offsets. The exact reason for its amplitude to not be recovered correctly is subject of ongoing research. Figure 5 also exhibits arrivals which were not reconstructed, shown under the dashed black line and above the direct wave arrival. These are  $S$ - $P$  converted waves that are muted by the windowing operator  $\theta(t + t_d^S(\mathbf{x}_0, \mathbf{x}_F))$  at the first step of each iteration (Eq. (22)) which precludes the appearance of any wave arrival before the direct wave.

Figures 6 and 7 demonstrate that many events were also recovered with comparable amplitudes to the directly modeled Green's functions. These seismograms have had a gain of  $e^{4t}$  applied to them in order to make later arrivals visible. In Fig. 6 we observe that a number of these events were recovered with equal amplitude, while some of them have been slightly attenuated. The amplitudes obtained in  $S$ -wave autofocusing are even more precise, as evidenced in Fig. 7.

In summary, the set of Figures 4, 5, 6 and 7 show that elastic autofocusing, while not perfectly accurate under the simplifying assumptions introduced in the Section II C, can still perform well with correct kinematic and amplitude recovery of many wave arrivals.

#### IV. CONCLUDING REMARKS

We present a single-sided representation theorem relating Green's functions of the elastodynamic wave equation to focusing functions of the same equation. By assuming that a focusing function in an elastic medium can be represented by a direct component and a succeeding scattered coda, this representation theorem is used to derive a 3D Marchenko equation for elastic wavefields. The Marchenko equation is solved by an iterative scheme

that requires the direct wave from a virtual source in the subsurface, and reflections acquired only at the surface. This scheme, upon convergence, generates up- and down-going fields that can be combined to yield the Green’s function from a virtual source in the subsurface to the acquisition surface. In the derivation, we assumed the lack of evanescent waves when performing up/down decomposition of the wavefield, and further limited the applicability of the method by supposing that the focused wavefield can be described by a direct component followed by a coda. Nevertheless, experimental results show that elastic Green’s function can largely be recovered from single-sided data, in a similar way as for acoustic wavefields.

The theory of focusing has a wide range of applications that include medical ultrasound, nondestructive testing and the method can be of use for nonlinear elastic imaging [33] which takes advantage of nonlinear interactions such as multiple scattering from any point in the subsurface. Elastic autofocusing provides many of these interactions given only one-sided reflected wave data and modeled direct  $P$ - and  $S$ -waves.

## ACKNOWLEDGMENTS

The authors thank the Edinburgh Interferometry Project sponsors (ConocoPhillips, Schlumberger Gould Research, Statoil and Total) for supporting this research, and CAPES for sponsoring Carlos Alberto da Costa Filho (process number 0061/13–1).

## Appendix: Stationary Phase Analysis

Stationary phase analysis provides an intuitive framework to understand how the above iteration operates for specific arrivals that satisfy high-frequency approximations. The first theoretical justification for autofocusing in 2D acoustic media came from a stationary-phase analysis of  $P$ - $P$  reflections in a medium with dipping layers [12]. Pure-mode elastic reflections ( $P$ - $P$  and  $S$ - $S$ ) satisfy similar arguments, however an alternative analysis is necessary in order to understand how mixed-mode ( $P$ - $S$  and  $S$ - $P$ ) conversions are reconstructed in elastic autofocusing. We provide this latter analysis here for  $P$ - $S$  reflections.

Consider a 2D, isotropic, homogenous medium with two horizontal density contrasts, and constant  $P$ - and  $S$ -wave speeds  $c_P$  and  $c_S$ , respectively (Fig. 8). Since all recorded components (velocities and stresses) have the same kinematic behavior and only differ in

their radiation patterns, we consider only their kinematics, which will be denoted  $E_k^\pm$  for iteration  $k$  to simplify notation. Using a high-frequency approximation we write the first step of autofocusing, Eq. (22) in the frequency domain as:

$$E_0^+(x_0, x_F, \omega) = A_T(x_0, x_F, \omega) \exp \left\{ i\omega \frac{\|x_F - x_0\|}{c_P} \right\} \quad (\text{A.1})$$

for a virtual or desired source position  $x_F$ . Here  $A_T$  is an amplitude factor and  $E_0^+$  represents the time-reversed direct from  $x_F$  to  $x_0$  (dashed ray in Fig. 8). Likewise, we write Eq. (23) as:

$$E_0^-(x_0'', x_F, \omega) = \int_{-\infty}^{\infty} G^-(x_0'', x_0, \omega) E_0^+(x_0, x_F, \omega) \Big|_{z=0} dx_0 \quad (\text{A.2})$$

While the up-going field  $G^-$  contains all orders scattered waves, we consider only the contribution of singly-scattered  $P$ - $S$  reflections. In the case of a  $P$ - $S$  reflection at base of the  $n$ th layer we define its high-frequency approximation  $G_{PS}^{-(n)}$  (solid ray in Fig. 8 for  $n = 2$ ) by

$$G_{PS}^{-(n)}(x_0'', x_0, \omega) = A_{PS}(x_0'', x_F, \omega) \exp \left\{ -i\omega \left( \frac{\|x_0'' - \bar{x}(x_0'', x_0)\|}{c_S} + \frac{\|\bar{x}(x_0'', x_0) - x_0\|}{c_P} \right) \right\} \quad (\text{A.3})$$

where  $\bar{x}$  is the point where the reflection occurred. Substituting Eqs. (A.1) and (A.3) into Eq. (A.2), we obtain

$$E_0^-(x_0'', x_0, \omega) = \int_{-\infty}^{\infty} A_{PS} A_T \exp \{ -i\omega \phi(x_0) \} \Big|_{z=0} dx_0 \quad (\text{A.4})$$

where

$$\phi(x_0) = \frac{\|x_0'' - \bar{x}\|}{c_S} + \frac{\|\bar{x} - x_0\|}{c_P} - \frac{\|x_F - x_0\|}{c_P} \quad (\text{A.5})$$

A stationary-phase evaluation of the integral assumes that the largest contribution to this integral comes from points where the integrand phase is stationary [32], that is, when its derivative  $\frac{d\phi}{dx_0}$  vanishes. This occurs when

$$0 = \frac{x_0'' - \bar{x}}{c_S \|x_0'' - \bar{x}\|} \left( -\frac{d\bar{x}}{dx_0} \right) + \frac{\bar{x} - x_0}{c_P \|\bar{x} - x_0\|} \left( \frac{d\bar{x}}{dx_0} - 1 \right) + \frac{x_F - x_0}{c_P \|x_0 - x_F\|}$$

or,

$$0 = \frac{\sin \psi_R}{c_S} \left( -\frac{d\bar{x}}{dx_0} \right) + \frac{\sin \theta_I}{c_P} \left( \frac{d\bar{x}}{dx_0} - 1 \right) + \frac{\sin \theta_T}{c_P} \quad (\text{A.6})$$

After applying Snell's law,  $\frac{\sin \psi_R}{c_S} = \frac{\sin \theta_I}{c_P}$ , the terms containing  $\frac{d\bar{x}}{dx_0}$  vanish, yielding the following equality:

$$\frac{\sin \theta_I}{c_P} = \frac{\sin \theta_T}{c_P} \quad (\text{A.7})$$

This relation states that the points  $x_0^{*(n)}$  which contribute the most energy to the integral in Eq. (A.2) is where the ray path of the reflection at the base of the  $n$ th layer aligns the direct wave ray path (Fig. 9).

For layers below the virtual source, in the case  $n = 2$  the phase at  $x_0^{*(2)}$  can be written as

$$\phi(x_0^{*(2)}) = \frac{\|x_0'' - \bar{x}\|}{c_S} + \frac{\|\bar{x} - x_F\|}{c_P} \quad (\text{A.8})$$

which is the travel time of a  $P$ - $S$  converted reflection recorded at  $x_0''$  from a source at  $x_F$ . Figure 9a depicts this situation: at the stationary point, the phase and hence travel time of the time-reversed transmission (dashed black ray) will cancel with part of the  $P$ - $S$  reflection travel time (solid black ray) leaving only the travel time from the  $P$ - $S$  reflection from a source at  $x_F$ . The  $P$ - $P$  reflection is shown in Fig. 9b for comparison: note that the recovery of the  $P$ - $S$  reflection requires larger surface source-to-receiver offsets than that of a  $P$ - $P$  reflection recorded at the same receiver.

At this point of the iteration, there are 2 new arrivals per layer, corresponding to the  $P$ - $P$  and  $P$ - $S$  reflections. Those which correspond to layers above the virtual source are nonphysical, as their travel times do not equal that of any arrival in the Green's function we aim to reconstruct (Fig. 9c,d). Those corresponding to the layers below are physical: their travel times correspond to those of reflections in the Green's function from  $x_F$  to  $x_0$  (Fig. 9a,b).

The second iteration of autofocusing starts by constructing the new down-going field by windowing  $E_0^-$ , time-reversing it and subtracting it from  $E_0^+$  as detailed in Eq. (15). In acoustic autofocusing, the window removes from  $E_0^-$  all of the physical arrivals. It is designed this way because if they were to be convolved again with the reflectivity, they would generate nonphysical arrivals. It retains the nonphysical arrivals: when convolved with the reflectivity again, they will generate internal multiples [10].

While in elastic autofocusing we assume the window acts similarly, it might fail in two situations. First, a nonphysical arrival can have a travel time that is longer than that of the direct wave, and will be erroneously outside of the window. Also, as observed in the  $S$ -wave



autofocusing example below, physical arrivals can have a shorter travel time than the direct wave, and will be inside of the window. These will not appear in the reconstruction as they are treated as nonphysical, and will also generate spurious arrivals when convolved with  $G^-$  in the creation of  $E_1^-$ .

Nevertheless, if the arrivals are filtered correctly, then only the nonphysical contributions will be subsequently convolved with  $G^-$  to generate internal multiples. For reflections on the first layer, this is shown schematically in Fig. 10 for a fixed receiver  $x_0''$  almost directly above the virtual source  $x_F$ . Travel times on common sections of solid and dashed rays cancel to produce the kinematics of the direct  $P$ -wave (Fig. 10a,c) but also create, at least kinematically, the converted  $P$ - $S$  transmission (Fig. 10b,d).

The convolution with the reflections from the layer below the virtual source are shown in Fig. 11, albeit only with the nonphysical event exclusive to the elastic case. We observe that all second order internal multiples are reconstructed, including those that underwent conversions. In fact, all possible internal multiples from a  $P$ -wave source are kinematically constructed with only one nonphysical event; the other nonphysical event result from the  $P$  direct wave is necessary in order to obtain correct amplitudes.

At the end of the second iteration  $E_1^+$  consists of the time-reversed direct wave and the nonphysical arrivals;  $E_1^-$  consists of the true internal multiples (resulting from the convolution of the nonphysical arrivals), and the (time-reversed) nonphysical arrivals (created by the convolution with  $E_0^+$ ). Therefore, when we time-reverse  $E_1^+$  and sum it to  $E_1^-$  to recreate the Green's function in accordance with Eq. (18), the nonphysical arrivals vanish, and only the direct wave and the internal multiples remain.

- 
- [1] I. M. Gelfand and B. Levitan, *Izv. Akad. Nauk SSSR Ser. Mat.* **15**, 309 (1951).
  - [2] V. A. Marchenko, *Dokl. Akad. Nauk SSSR* **104**, 695 (1955).
  - [3] M. Fink, *IEEE Trans. Ultrason., Ferroelectr., Freq. Control* **39**, 555 (1992).
  - [4] M. Campillo and A. Paul, *Science* **299**, 547 (2003).
  - [5] K. Wapenaar, *Phys. Rev. Lett.* **93**, 254301 (2004).
  - [6] D.-J. van Manen, J. O. A. Robertsson, and A. Curtis, *Phys. Rev. Lett.* **94**, 164301 (2005).
  - [7] K. Wapenaar and J. Fokkema, *Geophysics* **71**, SI33 (2006).

- [8] J. H. Rose, *Phys. Rev. A* **65**, 012707 (2001).
- [9] J. H. Rose, *Inverse Probl.* **18**, 1923 (2002).
- [10] F. Brogгинi and R. Snieder, *Eur. J. of Phys.* **33**, 593 (2012).
- [11] D. Halliday and A. Curtis, *Geophysics* **75**, SA95 (2010).
- [12] K. Wapenaar, F. Brogгинi, and R. Snieder, *Geophys. J. Int.* **190**, 1020 (2012).
- [13] K. Wapenaar, F. Brogгинi, E. Slob, and R. Snieder, *Phys. Rev. Lett.* **110**, 084301 (2013).
- [14] C. A. da Costa Filho, M. Ravasi, G. Meles, and A. Curtis, *76th EAGE Conf. & Exhib.* (2014).
- [15] C. A. da Costa Filho, M. Ravasi, G. Meles, and A. Curtis, *SEG Expand. Abs.*, 4603 (2014).
- [16] R. L. Weaver and O. I. Lobkis, *Phys. Rev. Lett.* **87**, 134301 (2001).
- [17] A. Curtis, P. Gerstoft, H. Sato, R. Snieder, and K. Wapenaar, *The Leading Edge* **25**, 1082 (2006).
- [18] G. Schuster, *Seismic Interferometry* (Cambridge University Press, Cambridge, 2009) p. 258.
- [19] J. L. Thomas, F. Wu, and M. Fink, *Ultrason. Imag.* **18**, 106 (1996).
- [20] M. Tanter, J.-L. Thomas, and M. Fink, *J. Acoust. Soc. Am.* **103**, 2403 (1998).
- [21] N. Chakroun, M. Fink, and F. Wu, *IEEE Trans. Ultrason. Ferroelec. Freq. Contr.* **42**, 1087 (1995).
- [22] J. Behura, K. Wapenaar, and R. Snieder, *Geophysics* **79**, A19 (2014).
- [23] K. Wapenaar, J. Thorbecke, J. van der Neut, F. Brogгинi, E. Slob, and R. Snieder, *Geophysics* **79**, WA39 (2014).
- [24] A. E. H. Love, *A Treatise on the Mathematical Theory of Elasticity* (Cambridge University Press, 1906).
- [25] C. H. Chapman, *Fundamentals of Seismic Wave Propagation* (Cambridge University Press, 2004).
- [26] J. F. Claerbout, *Geophysics* **36**, 467 (1971).
- [27] B. Ursin, *Geophysics* **48**, 1063 (1983).
- [28] C. P. A. Wapenaar and A. J. Berkhout, *Elastic wave field extrapolation: Redatuming of single- and multi-component seismic data* (Elsevier Science Publ. Co., Inc., 1989).
- [29] G. L. Lamb, *Elements of Soliton Theory* (John Wiley & Sons Inc, 1980).
- [30] Y.-H. Pao and V. Varatharajulu, *J. Acoust. Soc. Am.* **59**, 1361 (1976).
- [31] M. Ravasi and A. Curtis, *Geophysics* **78**, S265 (2013).
- [32] N. Bleistein, *Mathematical Methods for Wave Phenomena* (Academic Press, Inc., 1984).

[33] M. Ravasi and A. Curtis, [Geophysics](#) **78**, S137 (2013).

FIGURES

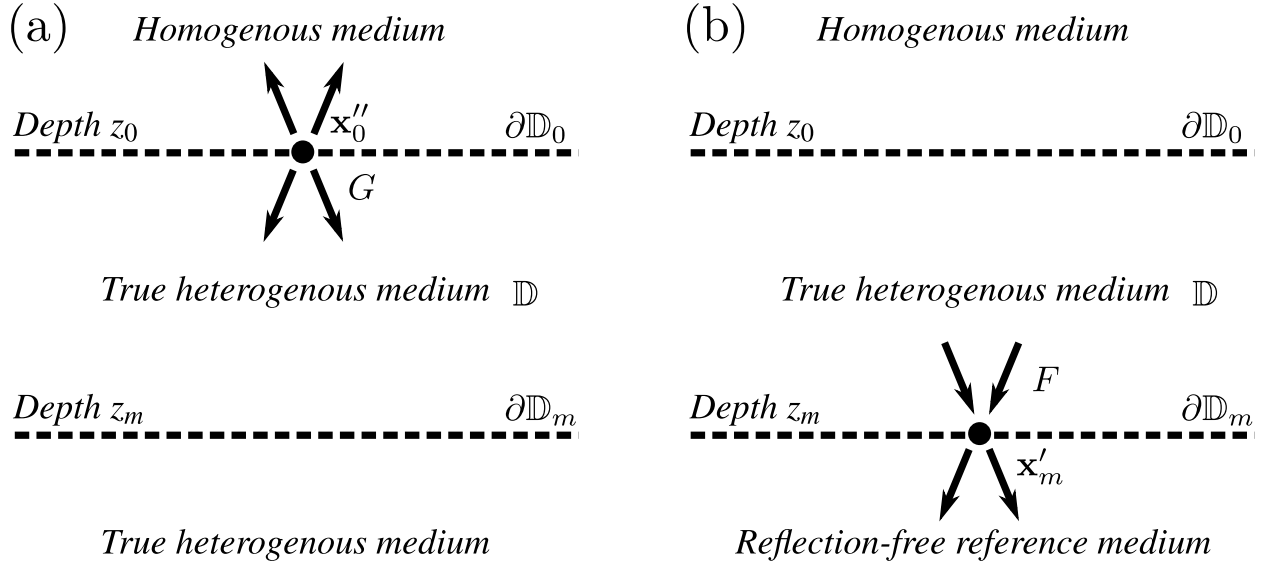


FIG. 1. Media in which (a) Green's functions and (b) focusing functions are defined.

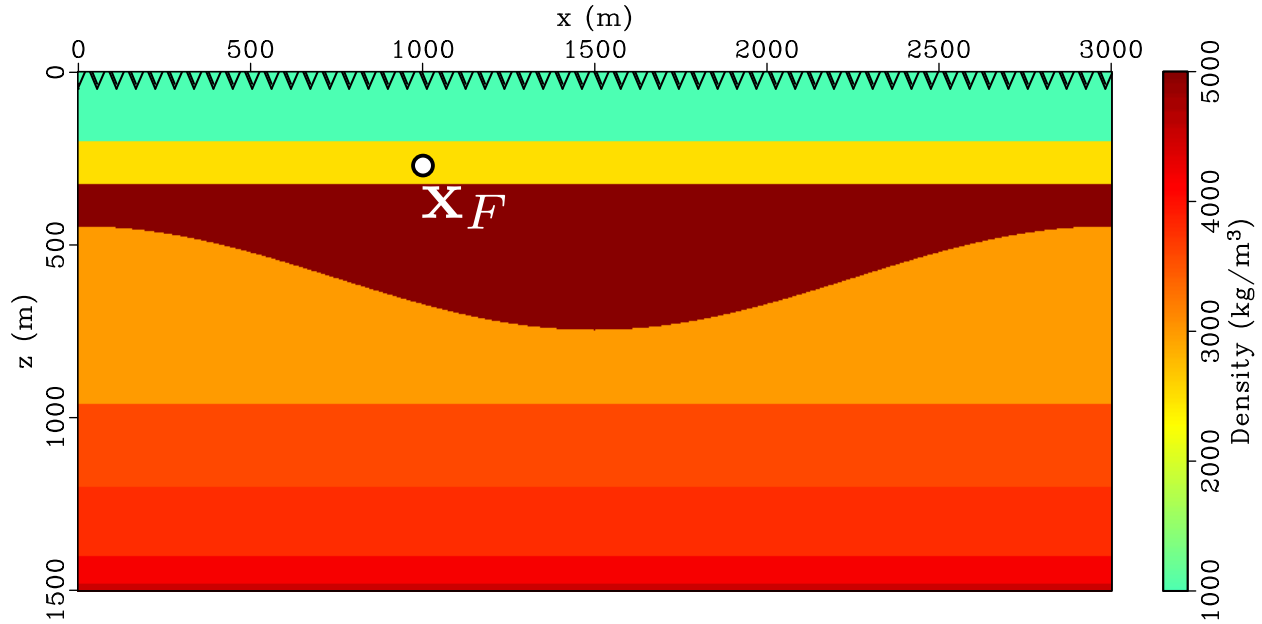


FIG. 2. (Color online) Density model with synclinal interface. Triangles represent both source and receiver positions on the acquisition surface; white circle represents the virtual source position  $\mathbf{x}_F$ .

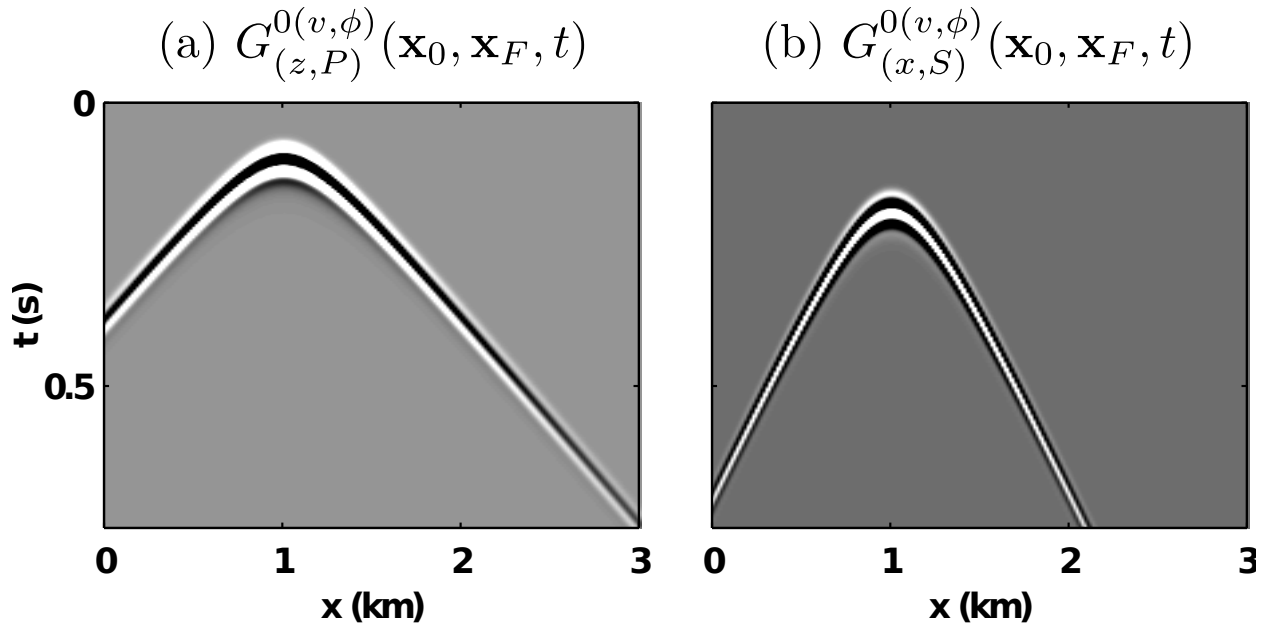


FIG. 3. Direct transmissions used to initialize  $\underline{\mathbf{E}}_0^+$ .

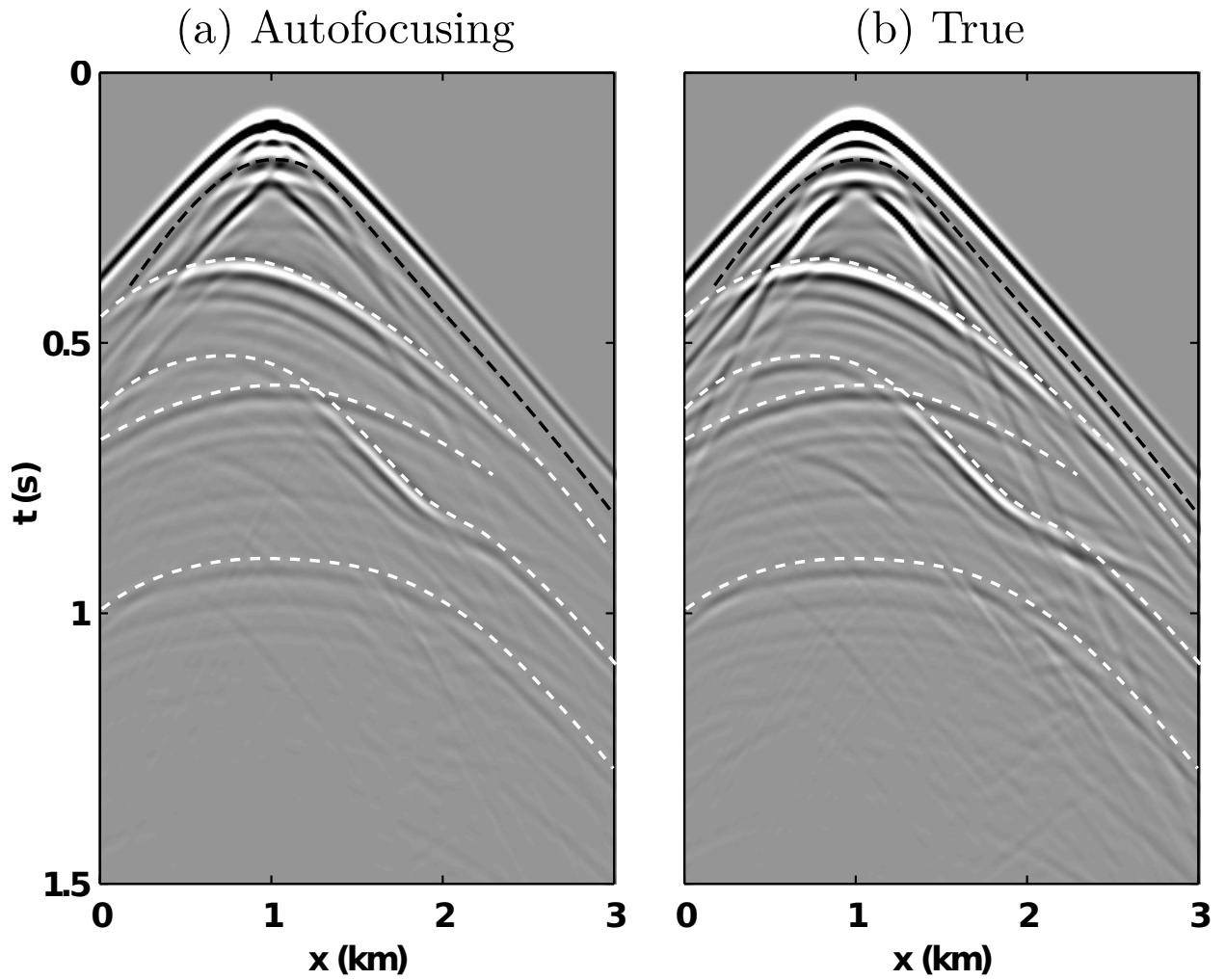


FIG. 4.  $v_z$  components of the Green's functions  $G_{(z,P)}^{(v,\phi)}(\mathbf{x}_0, \mathbf{x}_F, t)$  from a subsurface  $P$ -wave source in Fig. 3 from (a) elastic autofocusing and (b) direct modeling. Dashed white lines indicate arrivals common in the two gathers. Dashed black lines indicate arrivals that were not recovered.

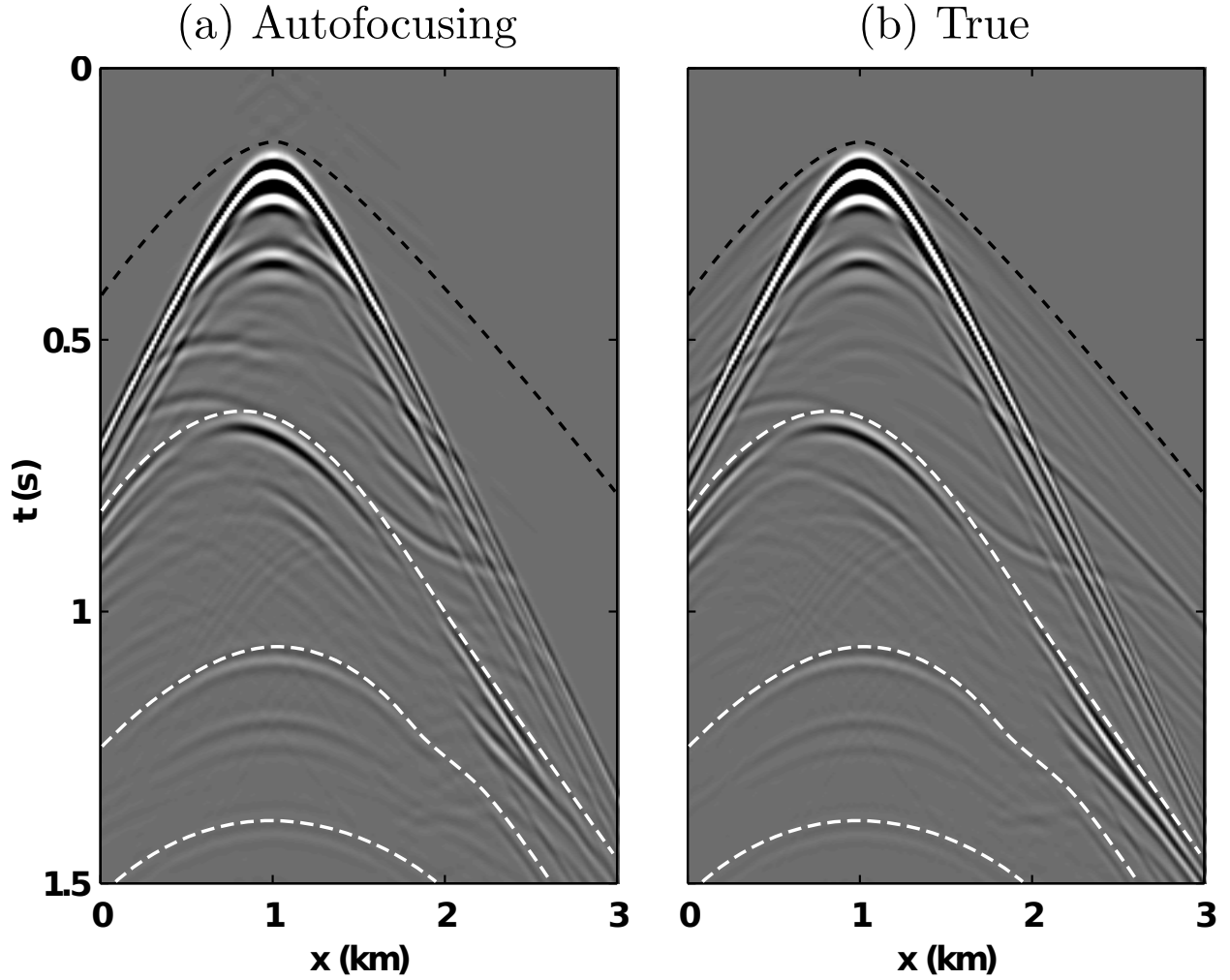


FIG. 5.  $v_x$  components of the Green's functions  $G_{(x,S)}^{(v,\phi)}(\mathbf{x}_0, \mathbf{x}_F, t)$  from a subsurface  $S$ -wave source in Fig. 3 from (a) elastic autofocusing and (b) direct modeling. Dashed white lines indicate arrivals common in the two gathers. Dashed black line indicates arrivals that were not recovered.

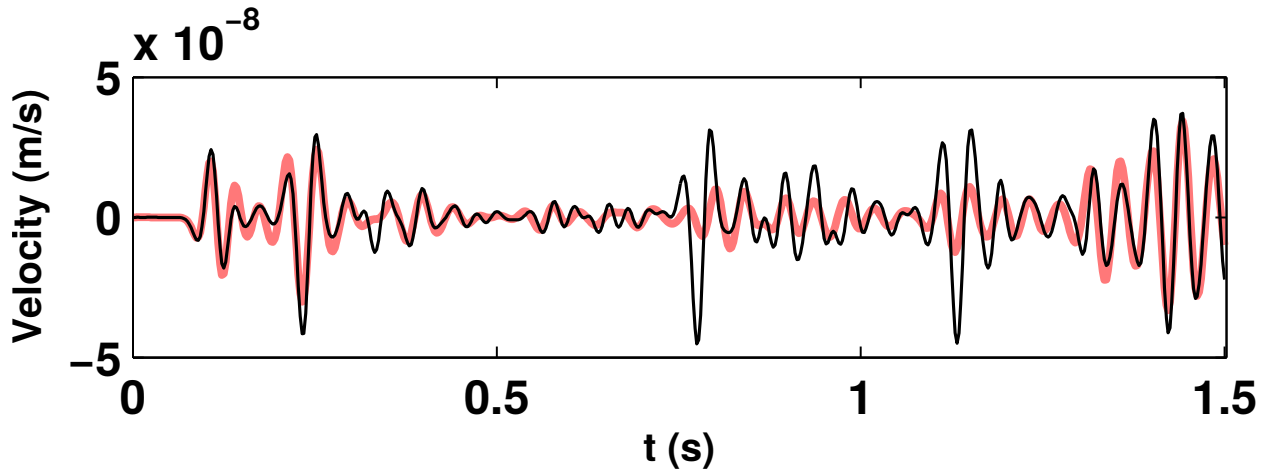


FIG. 6. (Color online) Seismogram from each image in Fig. 4 when  $\mathbf{x}_0 = (1 \text{ km}, 0 \text{ km})$ . The thin black line is the true velocity, and the thick pink (light gray) line is the recovered velocity. A gain of  $e^{4t}$  has been applied to enhance later arrivals.

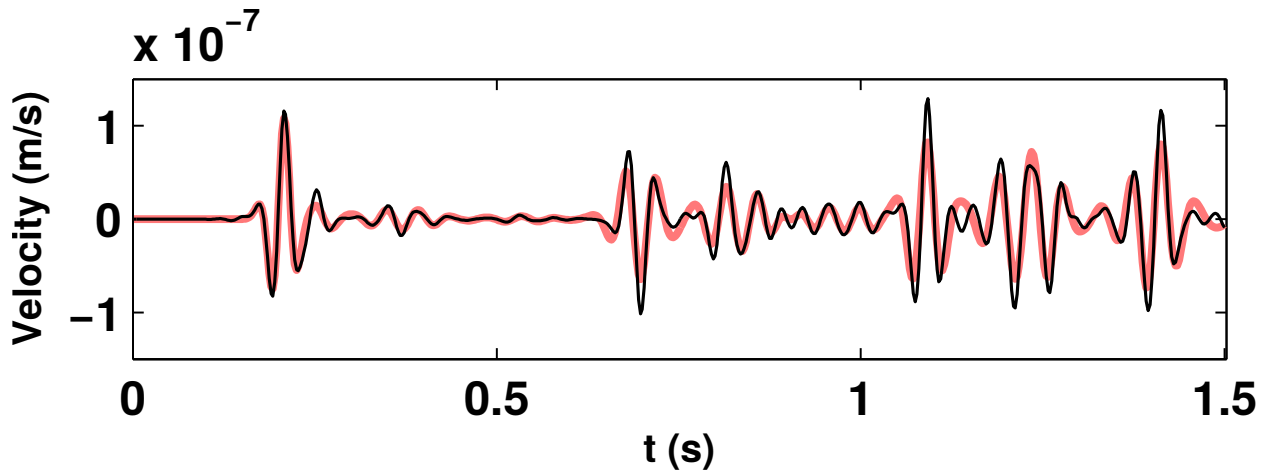


FIG. 7. (Color online) Seismogram from each image in Fig. 5 when  $\mathbf{x}_0 = (1 \text{ km}, 0 \text{ km})$ . The thin black line is the true velocity, and the thick pink (light gray) line is the recovered velocity. A gain of  $e^{4t}$  has been applied to enhance later arrivals.

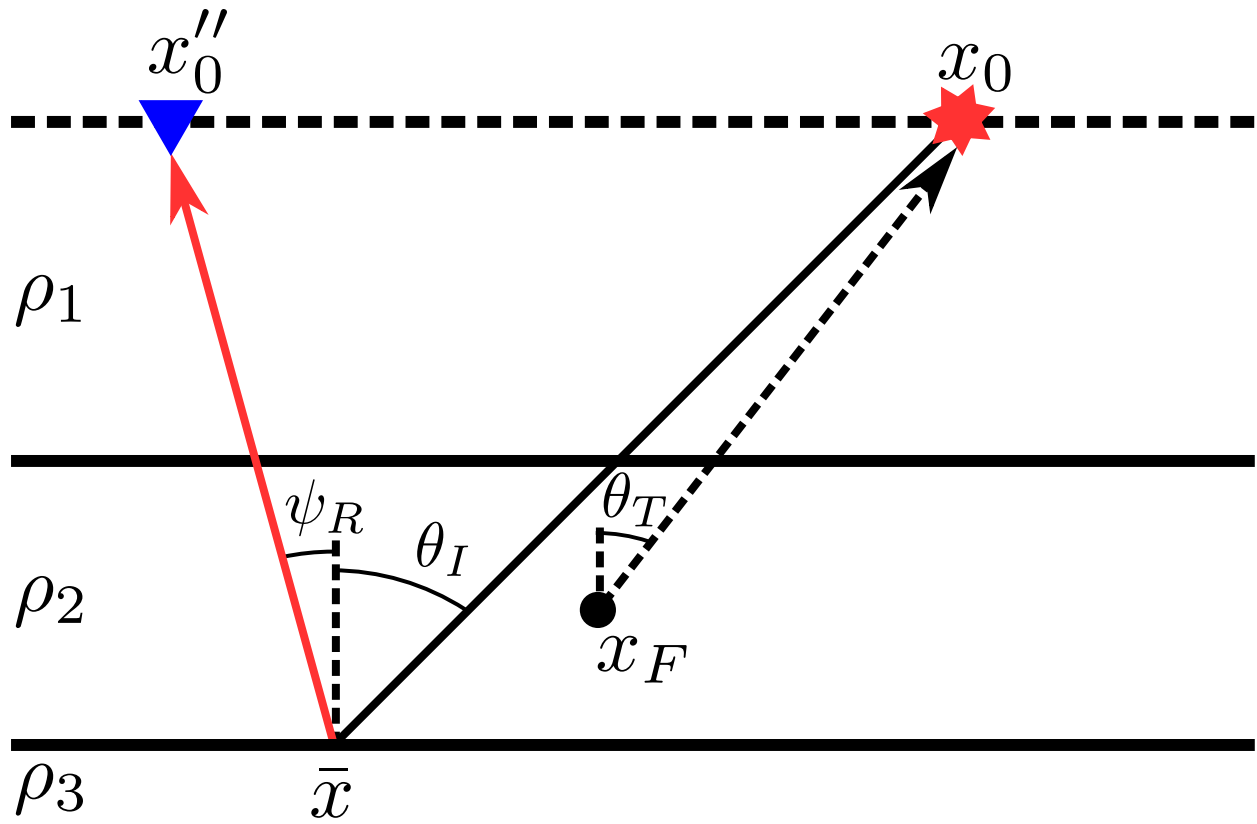


FIG. 8. (Color online) Horizontally layered medium. Black rays represent  $P$ -waves, and red (gray) rays  $S$ -waves. Dashed rays represent time-reversed quantities.



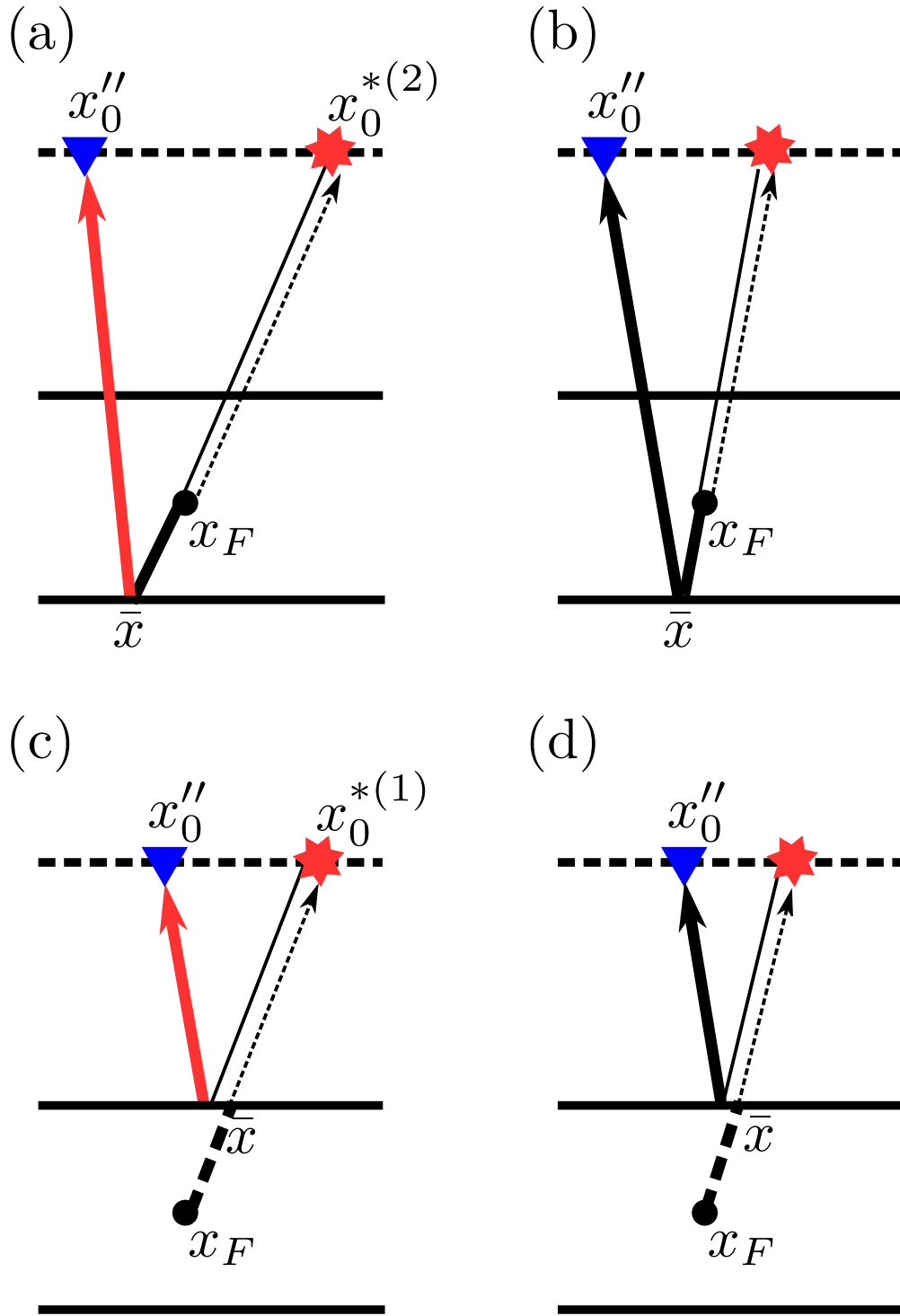


FIG. 9. (Color online) Stationary rays of first order reflections. Black rays indicate  $P$ -waves, and red (gray)  $S$ -waves. Dashed rays represent time-reversed quantities. Thicker arrows represent result of summing all travel times, as the thinner arrows cancel.

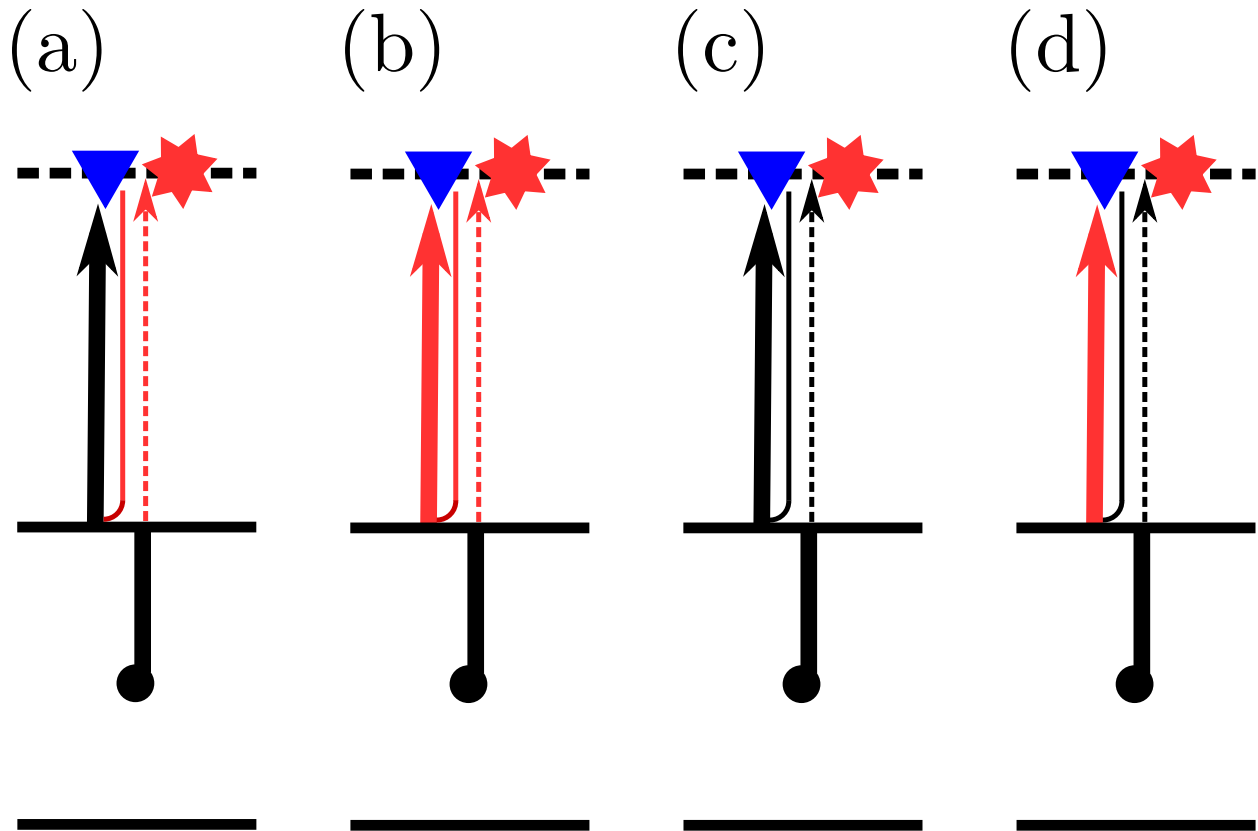


FIG. 10. (Color online) Stationary rays for first order reflections on the first layer at the second step of autofocusing. Here the equivalent diagrams to those in Fig. 9 are shown schematically with zero surface source-to-receiver offset for each component.

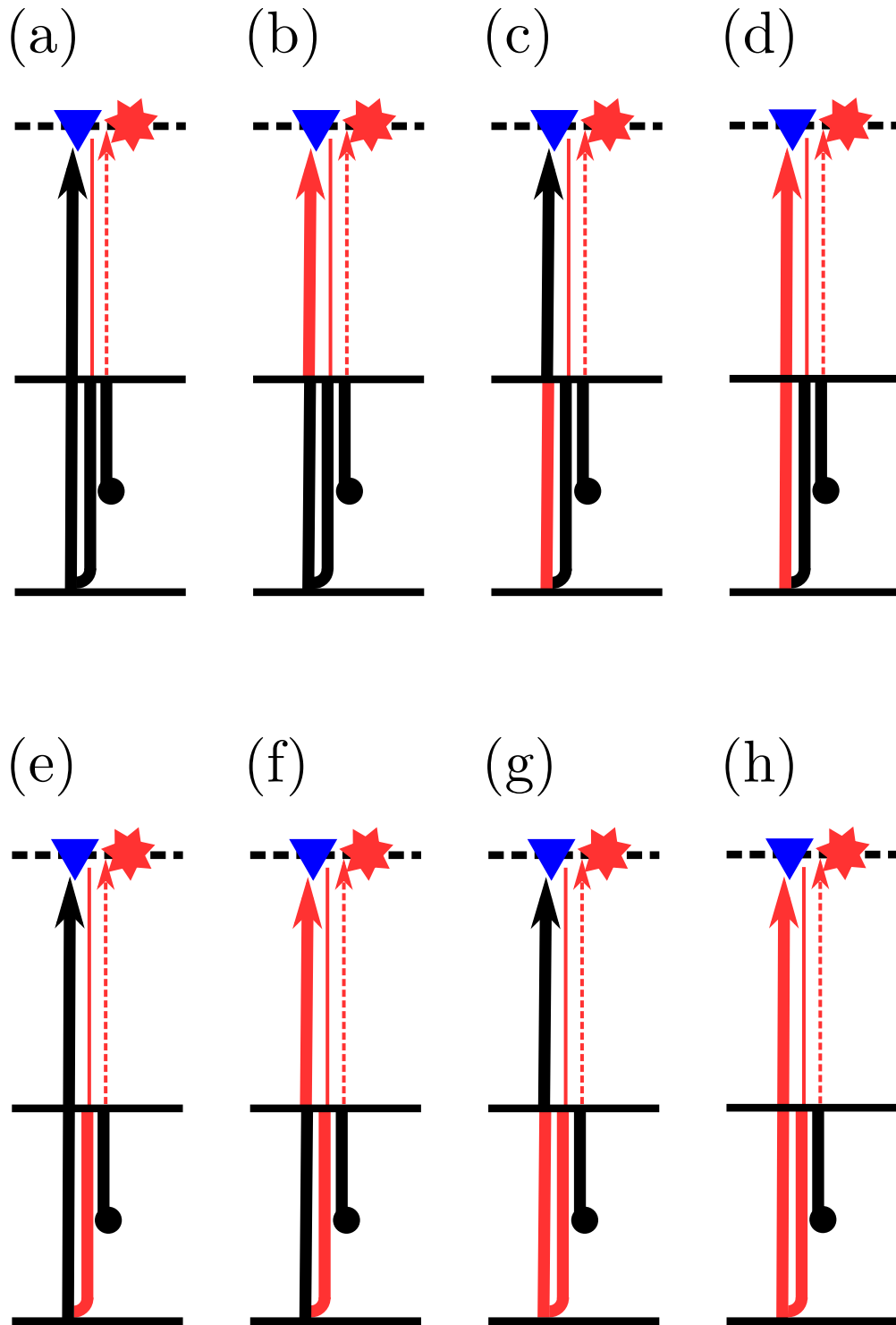


FIG. 11. (Color online) Stationary rays of first order reflections on the second layer at the second step of autofocusing. Here the equivalent diagrams to those in Fig. 9 are shown schematically with zero surface source-to-receiver offset for each components.